Audio Engineering Society
Convention Paper 9367
Presented at the 139th Convention
2015 October 29–November 1 New York, USA

Predicting the Acoustic Power Radiation from Loudspeaker Cabinets: a Numerically Efficient Approach

M. Cobianchi [1], Dr. M. Rousseau [1]

[1] B&W Group Ltd, Worthing, West Sussex, BN11 2BH, United Kingdom
mcobianchi@bwgroup.com, mrousseau@bwgroup.com

ABSTRACT

Loudspeaker cabinets should not contribute at all to the total sound radiation, but aim instead to be a perfectly rigid box which encloses the drive units. To achieve this goal, state of the art FEM software packages and Doppler vibrometers are the tools at our disposal. The modelling steps covered in the paper are: measuring and fitting orthotropic material properties, including damping; 3D mechanical modelling with a curvilinear coordinates system and thin elastic layers to represent glue joints; scanning laser Doppler measurements and single point vibration measurements with an accelerometer. Additionally a numerically efficient post-processing approach used to extract the total radiated acoustic power and an example of what kind of improvement can be expected from a typical design optimization are presented.

1. INTRODUCTION

While musical instruments often rely on a body which resonates purposefully to amplify the vibration produced by a string or a membrane, such as in a violin or a guitar, loudspeaker cabinets should not contribute at all to the total sound radiation, but aim instead to be a perfectly rigid box which encloses the drive units.

The aim of this project is to estimate the total radiated acoustic power output of a loudspeaker cabinet. The ultimate goal being to use finite element simulations to improve loudspeaker enclosure designs. The FEM package used was Comsol Multiphysics 5.0.

2. PROBLEM DESCRIPTION

2.1. State of the art

Lipshitz, Heal and Vanderkooy looked at the impact of cabinet vibration on the perceived sound quality (see [1]), concluding that in some cases cabinet mechanical resonances are audible. Olive's work on modification of timbre by resonance [2] also demonstrated that low amplitude resonances – typical of cabinet vibration – do affect sound quality. More recently Grande [3] came to the same conclusion, highlighting the impact of the cabinet on the time domain behaviour (spectral decay), while Bastyr and Capone measured the sound pressure level produced by a commercial floor standing loudspeaker with cabinet surfaces large enough to show

radiation levels comparable with that of the main drive units in the frequency range 100-300Hz [4].

This acoustic radiation is caused by two phenomena:

- The mechanical reaction force of the electrodynamic transducer (also referred to as the loudspeaker drive unit, or simply drive unit), causing the assembly to vibrate.
- The internal sound pressure – caused by the same drive unit back radiation, and the walls vibration excited by the first mechanism - which excites the cabinet walls and leaks by transmission. This is similar to the way a window or wall transmits noise.

The former is described in detail in [5] and in section 4 of this paper. The latter is not considered at the present stage, for the following reasons:

- Experimental evidence suggests that for this particular loudspeaker the mechanical excitation is the main source of cabinet radiation, at least for low frequencies. The definition of a low frequency region depends on the system size and is subject to interpretation, but is typically below 1000 Hz.
- The internal volume is filled with sound absorbing material, limiting the impact of internal acoustic standing waves. A preliminary study involving a fully coupled FEM model where both phenomena were taken into account, and the absorption material was modelled as an equivalent fluid, has shown indeed that except for a few peaks (near coincidence frequencies) the second phenomenon results in a radiated acoustic power 10 to 20 dB lower than the first.

As the acoustic output of most loudspeaker enclosure assemblies is low compared to the main transducer output, directly measuring it is complex and prone to error.

A possible hybrid method would rely on accurately measuring the outer surface walls velocity and on a FEM or BEM method to estimate the acoustic output in the far field, as investigated in [1] and [3]. Not only is this option difficult to implement in practice (ideally relying on 3D laser Doppler vibrometry) but it also requires a working prototype. This makes even more desirable the capability of accurately modelling inside a FEM package the cabinet vibration behaviour and compare different design options for a product optimisation. It`s also worth mentioning that prototyping curved panels requires an effort which is far greater than prototyping standard "box style" cabinets.

2.2. Device under study

The system considered in this study is the low frequency section of the loudspeaker system shown below:

Figure 1: loudspeaker system considered, B&W 800 Diamond

The transducers of interest are the two 10" units located in the lower enclosure. The low frequency section reproduces the low end of the audio spectrum and is fed through a passive electrical filter with the following transfer function:

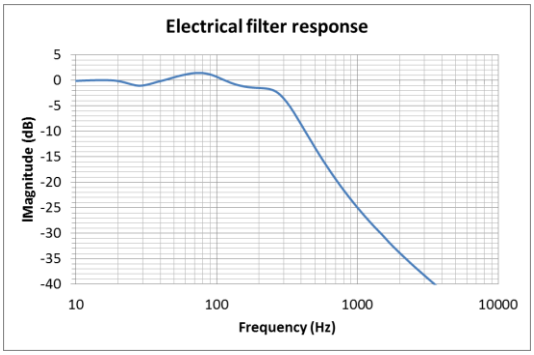

Figure 2: Electrical filter response of the crossover

The following work focuses on assessing the cabinet acoustic output in the 10 to 1600 Hz region. Above this upper frequency the input signal is strongly attenuated and therefore less critical.

3. MATERIALS

3.1. Cabinet

The enclosure is a complex assembly:

- curved wood external wrap,
- internal MDF stiffening panels (Matrix),
- Cast aluminum plinth on steel spikes.

For a full description of the material properties characterization, see [5].
Our material of choice for the curved cabinet wrap is birch plywood, a stack of wood sheets and binding resins, with the fibres alternatively orientated in each layer. The laminate is bent into shape (the "wrap") using heat and pressure.

As simulating each individual layer of wood sheets and resin is impractical for the complete cabinet assembly, an equivalent orthotropic bulk material was created. A different equivalent material was derived for each laminate configuration using a different number of layers, matching the first five bending modes of a sample plate measured with a laser Doppler vibro-meter with the predicted modes of the plate fem model.

Laminate Configuration	E_x (GPa)	E_y (GPa)	G_{xy} (GPa)	υ_{xy}
21 layers	8.45	10.75	1.16	0.03

Modes, exact solution (Hz)	Bulk approximation (Hz)
592 1225 1679 2154 2416	592 1226 1679 2156 2419

The results above clearly suggest that an orthotropic bulk formulation is suitable to accurately match the plate behavior.
The Young's moduli for the MDF panels were estimated using the same technique, assuming isotropic properties.

3.2. Glue joints

As replicating the exact glue joint geometry is unrealistic, a thin elastic layer formulation is used to approximate the joint's mechanical behaviour. As a truly viscoelastic behaviour cannot be simulated within a thin elastic layer, a single modulus and loss factor figure was chosen from the data below (figure 3). The interpolated values at 500Hz were used.

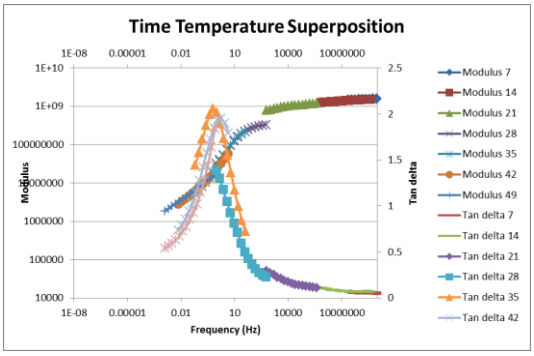

Figure 3: glue dynamic modulus (in Pa) and loss factor (tan delta)

A separate fem model was constructed to validate this approach. Two different glue joints were used in this assembly:

- Matrix to matrix panels: a dove tail construction is used with 0.5mm clearance between parts. The glue bead is applied on the outside.
- Matrix panel to curved wrap: a 10mm deep groove is machined in the wrap with a 0.5mm glue layer.

The dove tail details are shown below:

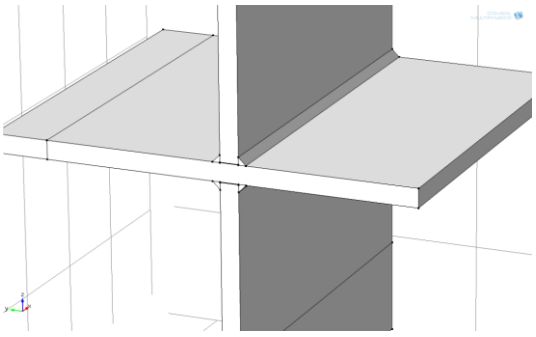

Figure 4: matrix to matrix glue joint

In order to assess the matrix to matrix glue joint impact, the small assembly shown in figure 4 was simulated and the first six eigenfrequencies compared to a perfectly solid joint (no clearance or glue). An average glue bead width of 2mm was found on real cabinets joints, thus the model has used a constant prismatic bead with 2mm side.

Rigid construction	2mm wide glue joint	Error (%)
1035 Hz	999 Hz	3.5%
1177 Hz	1137 Hz	3.4%
1451 Hz	1375 Hz	5%
1578 Hz	1504 Hz	4.7%
1690 Hz	1643 Hz	2.7%
2063 Hz	1990 Hz	3.5%

As the glue joint construction only has a marginal impact on the mode values, a rigid construction is used in the complete assembly model.

The matrix to wrap groove is shown below:

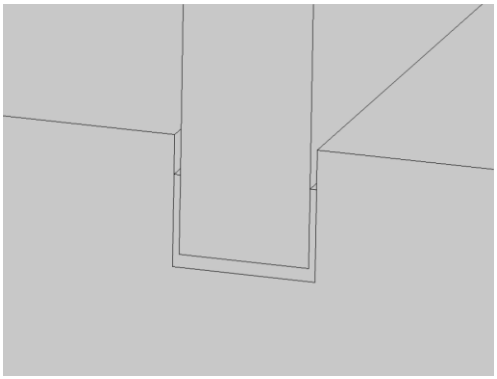

Figure 5: wrap to matrix groove

Again, an eigenfrequency analysis was performed on a small section in order to estimate the impact of the glue joint:

Rigid assembly (perfect fit) modes	Glue joint modes
474 Hz	409 Hz
1066 Hz	981 Hz
1538 Hz	1435 Hz
2561 Hz	2389 Hz
2692 Hz	2444 Hz

This time the impact is significant; a thin elastic layer formulation was then used to replicate the glue impact.
As a starting point the equivalent stiffness in compression and shear of a 0.5mm thick layer of glue was used. These values were then adjusted – as the glue only covers 70% of the groove sides – in order to get a close match for the first six eigenfrequencies:

Thin elastic layer modes	Glue joint modes
424 Hz	409 Hz
996 Hz	981 Hz
1411 Hz	1435 Hz
2351 Hz	2389 Hz
2510 Hz	2444 Hz

The approximated stiffness values are subsequently used in the complete assembly.

3.3. Other properties

The other materials used in the assembly are:

- Aluminium plinth and loudspeaker unit chassis.
- Soft iron and Neodymium loudspeaker motor.

All metallic parts use the COMSOL material library default material properties. Neodymium parts, having a negligible impact on the system mechanical modes, use soft iron elastic properties.

4. NUMERICAL MODEL

Since the cabinet is composed of a curved wrap which constitutes the lateral wall, a curvilinear coordinate system was implemented to project the orthotropic properties of plywood along the curved surface:

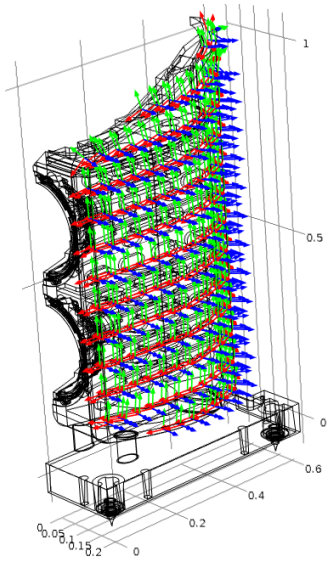

Figure 6: wrap curvilinear coordinate system

The joints between the matrix panels and the bottom, top, front and wrap were simulated through the use of the "Thin Elastic Layer" boundary condition described above.
Following this, a 3D model of the cabinet was simulated first as a vibro-acoustic coupled problem (structural mechanics plus acoustics) terminating the air domain with Perfectly Matched Layers boundary conditions to simulate a free field regime [6], and including only the

exterior air domain in the modelling to avoid the interior acoustic field to affect walls vibration.

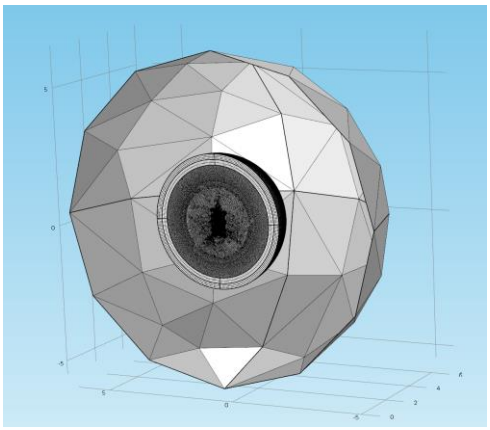

Figure 7: Coupled problem mesh

Then the same 3D model was solved only for the structural mechanics physics.

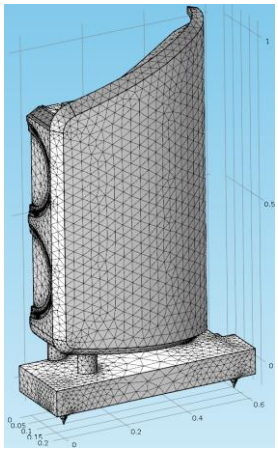

Figure 8: Structural mechanics model mesh

Due to the left-right symmetry of the system, only half of the structure was used.

5. POST-PROCESSING

5.1. Electromechanical coupling

5.1.1. Theory

Our forced response simulation assumes a unitary force input of 1[N] applied to the magnetic motor. The reality is more complex as the force generated by the transducer motor system and applied to the structure is highly frequency dependent. This relates to the electromechanical transfer function between the input electrical voltage applied across the transducer terminal and the motor output force. This transfer function was analyzed using a linear lumped parameter electromechanical model which describes the transducer cone (assumed infinitely rigid) and the electrical impedance of the coil. This approach allows us to simply post-process the model output quantities with the estimated transfer function.

This lumped parameter approach is well documented (see [7] to [9]) but normally used to describe the low frequency behaviour of loudspeakers.

As the frequency range considered in this case was limited (up to 1600Hz) the loudspeaker cone behaves like a perfect piston, making the lumped parameter assumption valid.

Considering the simple case of a single loudspeaker drive unit in free air (no enclosure), the cone/coil assembly movement is described by the following equations (equation of motion and Ohm's law):

$$M_{MS}\ddot{x} + \mathrm{K}_{MS}\, x + \mathrm{R}_{MS}\, \dot{x} = Bli \qquad \textbf{Equation 1}$$

$$Z_E i + Bl\dot{x} = U \qquad \textbf{Equation 2}$$

With $x, \dot{x}, \ddot{x}$ the cone displacement, velocity and acceleration relative to the magnetic motor, U the input voltage across the drive unit terminals, M_{MS} the cone moving mass, K_{MS}, R_{MS} the drive unit suspension stiffness and viscosity and Z_E the fixed coil electrical impedance.

From the above linear equations, calculating the system voltage to cone displacement and voltage to current transfer functions is trivial ([8]).

The forces applied to the magnetic motor are as follows:

- Direct coil reaction force

$$F_1 = -Bli = -\frac{BlU}{Z} \qquad \textbf{Equation 4}$$

with Z the system electrical impedance

- Reaction force of the mechanical suspension

$$F_2 = K_{ms}x + R_{ms}\dot{x} \qquad \textbf{Equation 5}$$

The total force applied to the assembly is therefore:

$$F_T = F_1 + F_2 \qquad \textbf{Equation 6}$$

5.1.2. Validation

The Klippel Distortion Analyzer system, measuring the transducer current transfer function, displacement transfer function and electrical impedance provides an estimation of all the physical parameters ($M_{MS}, K_{MS}, R_{MS}, Z_E$). The details of this estimation are outside of the scope of this paper.

In order to validate this lumped parameter approach, a simple case was used, based around a single loudspeaker drive unit suspended on rubber bands in order to simulate a free air condition. The resonance frequency of this mass-spring assembly is around 4Hz, outside of the frequency band of interest. The motor acceleration was measured for a constant voltage input and compared to the predicted force and acceleration given by the equation of motion:

$$F_T = m\ddot{x}_{motor} \qquad \textbf{Equation 7}$$

With m the motor total mass.

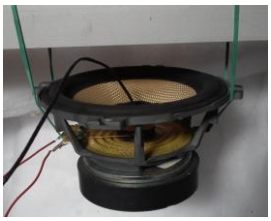

Figure 9: accelerometer mounted on the dust cap

The total force applied to the magnet assembly is estimated using the approach described above. Both forces are displayed in Figure 10 for a 4V input. As expected, the suspension reaction force only marginally impacts the total force above the transducer resonance frequency (50Hz). Above this frequency the cone is effectively decoupled from the magnet assembly.

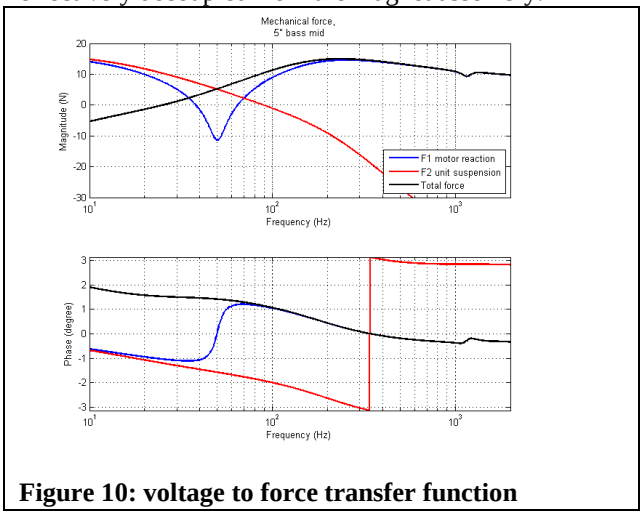

Figure 10: voltage to force transfer function

The measured acceleration is shown below with the estimated result:

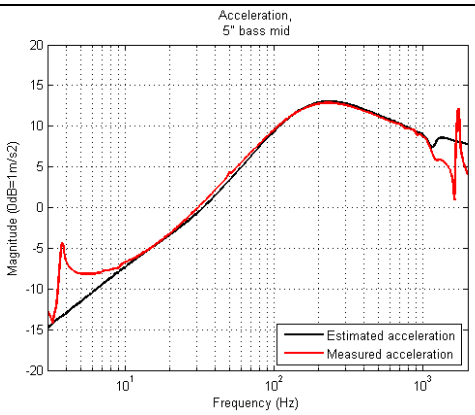

Figure 11

The rubber band mounting resonance is clearly visible just below 4Hz. Above 1KHz, various mechanical resonances (cone break-ups) invalidate the results.

In the region of interest (10Hz to 1000Hz) the force estimation matches the measured results within ±5% (0.5 dB).

5.1.3. Transducers used in cabinet assembly

The transducers used in the final assembly were based on two 10 inch bass units with the cone removed (see below) in order to limit the amount of radiated sound and the related acoustic excitation of the cabinet walls.

Using this method, the assembly is only mechanically excited by the motor reaction force, as in the simulation.

The derived voltage to force transfer function derived using the method used in 5.1.1 is shown below:

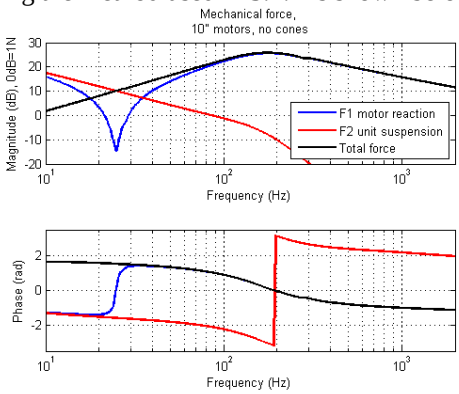

Figure 12: voltage to force transfer function for the cabinet transducers

The force transfer function, together with the crossover transfer function, were applied to the acceleration plots presented in section 6. (where they were compared with direct measurements on prototypes), but were not used for the acoustic power computation described in the next section, where a constant unitary force is applied over the entire frequency range of interest.

5.2. Acoustic power computation

5.2.1. Theory

Since the radiation from the cabinet is treated as a detrimental contribution to the total acoustic field, but at the same time the complex interaction of this radiation with the acoustic environment in which the loudspeaker is expected to work in is not predictable, the most useful quantity to synthetically describe this output is the acoustic power, used in the same manner as in noise sources characterization like engines, turbines, etc.
This approach provides two benefits:
-only a single quantity, function of frequency, is used to characterize a design, making it easy to compare many different designs;
-the result depends on the source features alone, and is not affected by the acoustic environment, like close boundaries and obstacles.

It`s worth noting that the theory and the modelling approach described below can also be successfully applied if and when the acoustic field inside the cabinet is taken into account and leaks by transmission need to be included.

The acoustic power (AP) can be calculated by integrating the acoustic intensity on a surface S enclosing the source [10]. By definition, the acoustic intensity is the product of pressure and particle velocity in the medium.

$$\mathrm{AP}=\int_S I_n dS = \int_S \frac{1}{2}\mathrm{Re}(pv_n{}^*)dS \quad \textbf{Equation 8}$$

To compute the acoustic power, the values of pressure and particle velocity on S have then to be known. Assuming that it is in the far field, i.e. far enough from the radiating structure such that the plane wave approximation applies, the particle velocity can be replaced by

$$v_n = \frac{p}{\rho c} \quad \textbf{Equation 9}$$

With ρ the air density and c the speed of sound in air.

Preliminary convergence studies have shown that for cylindrical sources a spherical surface radius that is 14 times the source radius results in an error for the Acoustic Power Level within 0.5dB.

The acoustic power can thus be written as a function of the pressure alone as below

$$\mathrm{AP}=\frac{1}{2}\int_S \frac{pp^*}{\rho c}dS \quad \textbf{Equation 10}$$

The most accurate numerical model to predict the pressure in the far field for a generic structure would be the vibro-acoustic coupled model (structural mechanics plus acoustics). Since only the structural excitation is of interest for this paper, the interior air volume was excluded from the modelling to avoid acoustic standing waves from affecting the vibration excited by the drive units reaction forces. This coupled approach is extremely demanding in terms of computation time and memory, restricting greatly the maximum frequency for which the total number of degrees of freedom (mainly affected by the acoustic domain meshing at high frequencies) is compatible with the available RAM of the computer the model runs on.

For radiating structures where the moving mass is much higher than the air load mass, it can also be assumed that the air inertial load has a negligible effect on the vibration, thus a structural mechanics model is able to fully describe the vibro-acoustic behaviour without the necessity of solving a coupled problem taking into account the air load. This approach would be definitely preferable because the model size is scaled down considerably as only the radiating structure is meshed

and only the structural degrees of freedom are solved for.

To compute the far field acoustic pressure from the radiating structure surface velocities, three numerical methods are available [10]:
-the Boundary Element Method, the most accurate but computationally demanding, requires the use of external code on top of the main software used in this paper for the FEM solution of the structural mechanics side;
-the Rayleigh integral, a widely used and well known approximation for radiation from shallow structures in an infinite baffle;
-the High Frequency BEM, a simplified BEM formulation valid at high frequencies, where the radiation impedance at the boundary is comparable with the characteristic impedance of the medium.

The High Frequency Boundary Element Method as described in [10] is basically "correcting" the Rayleigh integral through scaling the surface velocity of a point Q by the scalar product of the surface normal n and a unity vector, parallel to r, which is connecting Q with the observation point P where the pressure is computed. This allows to take into account the curvature of the radiating surface.

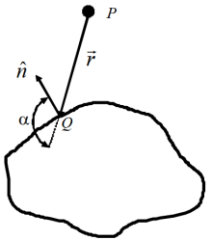

This approach is then ideal for optimization problems of non-shallow structures because it`s fast and simple enough to be implemented directly within the FEM software.

5.2.2.Validation

To keep the complexity of the model and the size of the mesh to a minimum, the validation was conducted for a simplified version of a new concept cabinet similar to the one shown in Figure 17 in two stages. This cabinet has a shape close to a hemi-cylinder, where the plinth, the drive units and all small parts were removed, and the structure was excited applying a boundary load along the interface between the drive units chassis and the front baffle.

Coupled Model

Acoustic Power Level predictions were compared for a fully coupled vibro-acoustic model, where the acoustic intensity is integrated over a spherical surface within the air domain and enclosing the source. The air domain radius is 8.5 times the cabinet radius and 2.5 times the cabinet height.
The cabinet walls surface velocities were used for the Rayleigh integral and the HFBEM approximation used to estimate the far field sound pressure on a spherical surface which has a radius that is 23 times the cabinet radius and 6.7 times the cabinet height. The results are shown in figure 13.

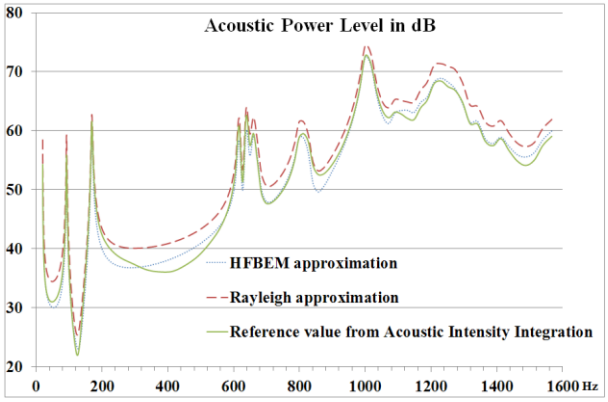

Figure 13, Acoustic Power Level versus frequency

The total error for the Rayleigh and HFBEM acoustic power level predictions using as the reference the acoustic intensity integration is compared in figure 14.

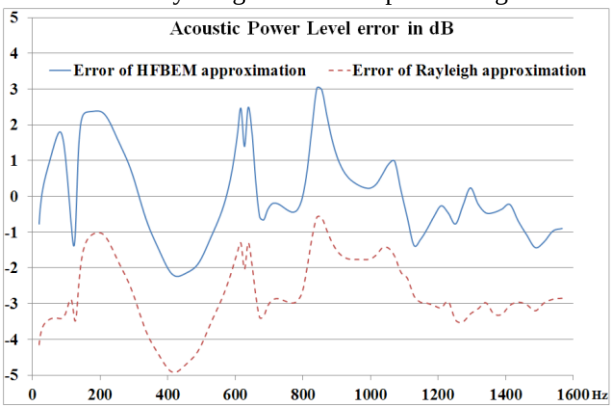

Figure 14, Acoustic Power Level error versus frequency

The Rayleigh approach results in a maximum error of 4.9dB, while the HFBEM approach results in a maximum error of 3dB, confirming the validity of the

HFBEM approach to evaluate the Acoustic Power Level for non-shallow structures with a reasonable accuracy.

Purely Structural Model

Acoustic Power Level predictions were then computed solving for the structural mechanics physics alone, disregarding the air domain and thus the air load, using the cabinet walls surface velocities for the Rayleigh integral and the HFBEM approximation to estimate the far field sound pressure on the same spherical surface used for the coupled model.
The results are shown in figure 15: the curves are perfectly overlaid, with a maximum error of 0.4dB at 827Hz, 1017Hz and 1230Hz.

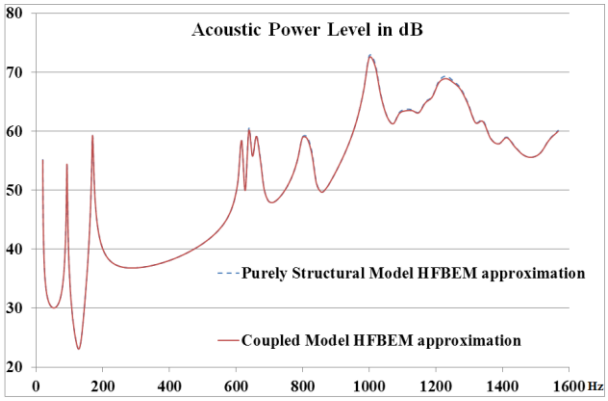

Figure 15, Acoustic Power Level versus frequency

The total error of the structural model HFBEM acoustic power level predictions using as the reference the coupled model HFBEM value and the acoustic intensity integration is plotted in figure 16, and follows of course the results of figure 15.

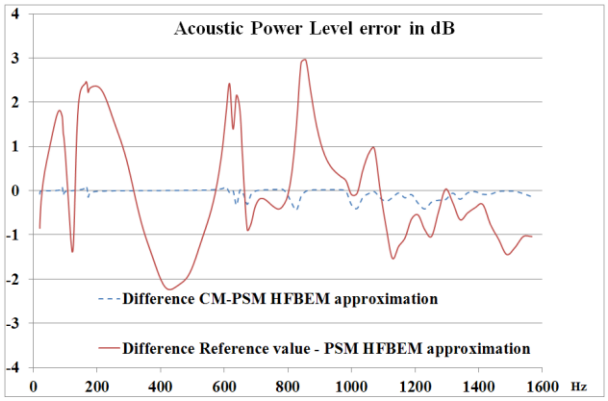

Figure 16, Acoustic Power Level error versus frequency

Computational Efficiency

The computation time for a frequency resolution of 40 points per octave, resulting in 255 frequencies in the frequency range 20-1600Hz, was 240 hours for the coupled vibro-acoustic model (6.3MDOF, segregated-iterative solver) and 3.5 hours for the purely structural model (343KDOF, MUMPS direct solver). Further optimization of the solver used for the structural model [5], resulted in a further reduction of the computation time to 1.7 hours. This means that for the same time required for one fully coupled model, 68 models can be run instead using the standard solver, or 141 models using the optimized solver, if the error shown above is considered acceptable.

Optimized Design

The computational efficiency of the simplified approach shown above allowed a large number of design iterations to be run starting from the 800 Diamond cabinet shown on the left of figure 17 to arrive at an optimized design, on the right, using a plywood matrix with steel brackets (shown in purple). The latter has achieved a reduction of the total number of modes in the cabinet and an acoustic power reduction in the most significant frequency range (taking into account the considerations in section 5.1 and the crossover transfer function which is rolling off at about 300Hz) of between 10 and 20dB (figure 18).

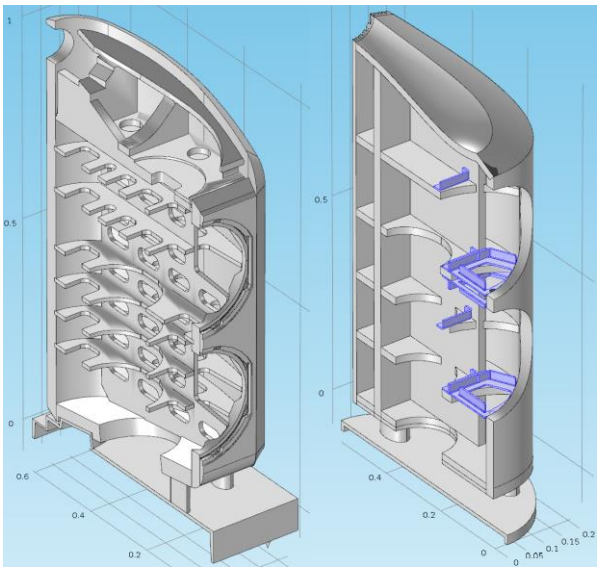

Figure 17: 800 Diamond cabinet geometry and new optimized cabinet design

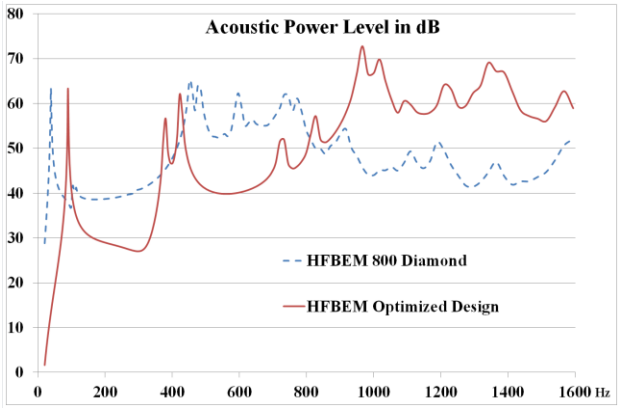

Figure 18: Acoustic Power Level versus frequency

6. EXPERIMENTAL RESULTS

An 800 Diamond purpose built cabinet with the drive units described in section 5.1.3 was driven while the velocity of each point on a user defined grid over the wrap and front baffle (the two largest radiating surfaces and thus the most important) were measured with a Polytec laser Doppler scanning system. The measured modal shape and frequency (left) are compared below to the predicted data (right) for the first relevant modes of the front baffle and wrap.

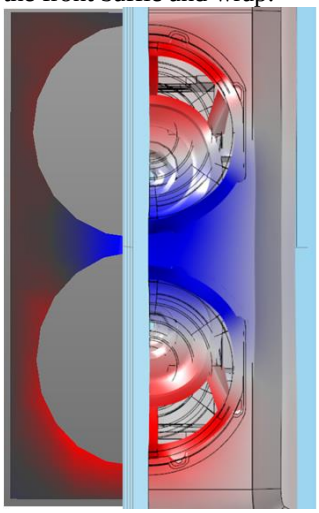

Figure 19: front baffle normal velocity at 222 Hz measured / 281 Hz predicted frequency

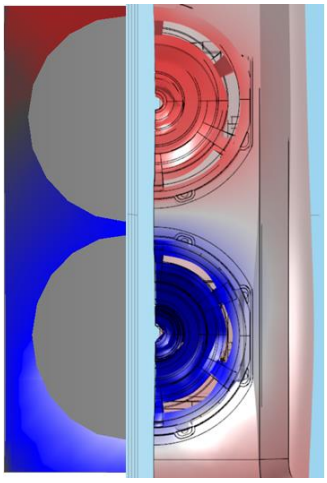

Figure 20: front baffle normal velocity at 313 Hz measured / 466 Hz predicted frequency

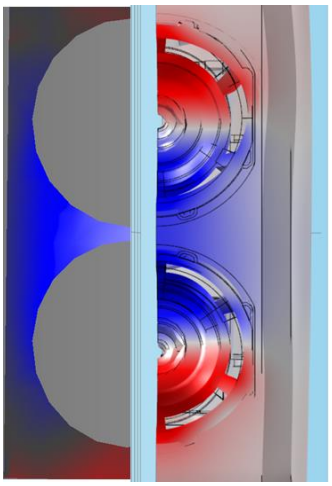

Figure 21: front baffle normal velocity at 603 Hz measured / 690 Hz predicted frequency

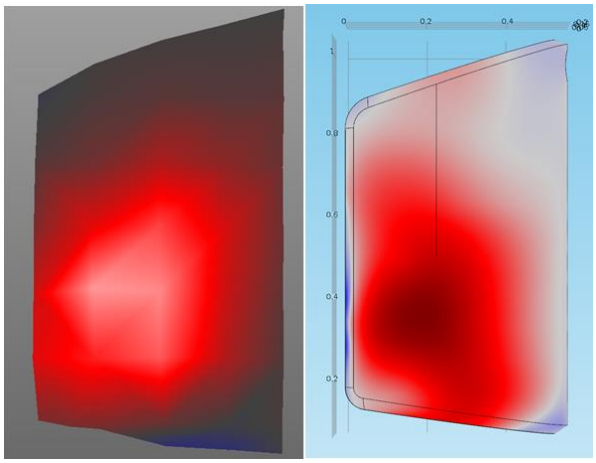

Figure 22: wrap normal velocity at 454 Hz measured / 502 Hz predicted frequency

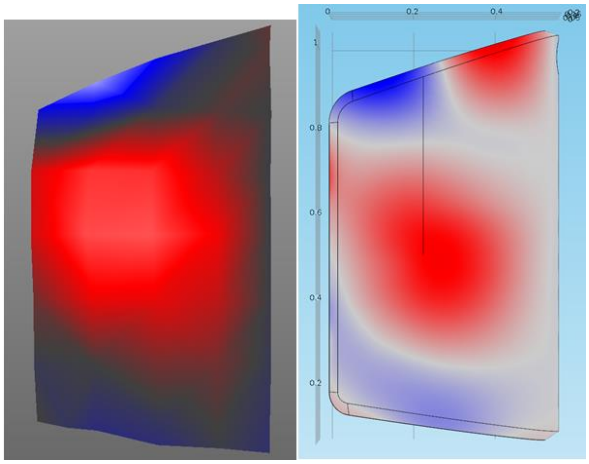

Figure 23: wrap normal velocity at 756 Hz measured / 801 Hz predicted frequency

The measured and predicted acceleration magnitude spectra were also overlaid for two critical locations (cabinet front baffle and middle of side baffle):

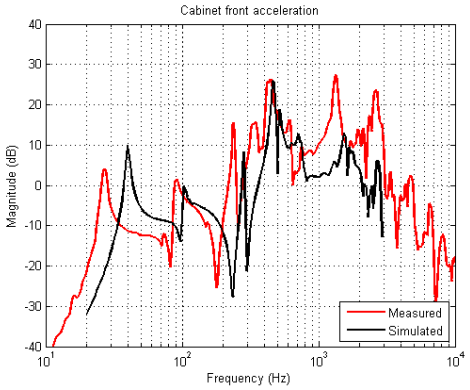

Figure 24: cabinet front acceleration

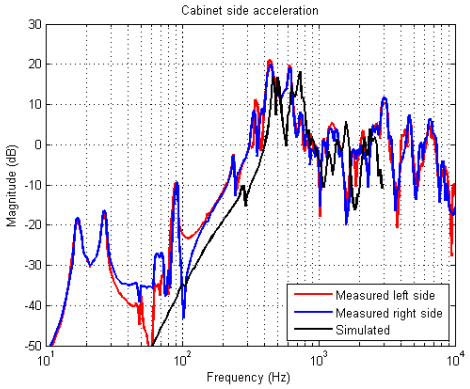

Figure 25: cabinet side acceleration

The following features are visible in the spectra in figures 24-25:

- Peaks below 90Hz are related to the rigid body motion of the enclosure on its spikes (acting like springs);
- The 90 Hz peak is a plate bending mode of the plinth;
- Peaks in the 250Hz to 900Hz region are complex modes related to the front baffle and side wrap.

The simulation was able to reproduce these three regions fairly well but systematically over-estimating the modes frequency values by 10 to 20%. Predicted peak amplitudes and Qs are realistic.

For the front baffle acceleration, the soft gasket coupling the drive unit chassis with the baffle is

responsible for the lower measured frequency of most baffle modes.

About the largest discrepancy for the wrap acceleration below 100Hz, the left to right symmetry assumption used was clearly not valid for the rigid body modes on the spikes – the left and right side measurements differ by up to 15dB. As each spike was terminated by a small 1mm spherical cap, obtaining a consistent mechanical interface with the floor below was difficult.

The most likely explanation for these discrepancies is the wood properties variation with temperature and among different batches. On top of this, the test cabinet tolerance stack up in the machining of the matrix joints and in the plywood wrap grooves used for the matrix coupling to the wrap are contributing to make the test cabinet 3D geometry slightly different from the theoretical 3D CAD data.

7. CONCLUSIONS

A complete loudspeaker enclosure model was constructed, including the use of orthotropic materials combined with a curvilinear coordinate system and hysteretic damping.
A very efficient computational approach for the radiated acoustic power level prediction based on the High Frequency BEM approximation has been compared with a more accurate but very time consuming coupled model, showing a maximum error of 3dB, and a design optimization was presented to show the kind of improvement which can be achieved.
Simulated accelerations show good agreement with measured results on a test cabinet; the model is able to accurately predict trends even if overestimating the resonance frequency values.
This model provides a valuable tool for designing improved loudspeaker enclosures, where the minimization of the cabinet radiation in terms of Acoustic Power output can be pursued by various means: moving the modes to a frequency range where damping material is most effective, moving them out of the audible frequency range, and modifying the modal shapes in order to minimize their radiation efficiency and thus the radiated sound pressure.

Future work should aim:
-to acquire more experimental data on different test cabinets to assess tolerances impact and thus improve the accuracy of the resonance frequency predicted values on the experimental side,
-to investigate the role of cabinet volume, alignment and port location, drive unit volume displacement and acoustic absorption material distribution in the cabinet radiation by acoustic transmission through the walls for different size cabinets.

8. REFERENCES

[1] Lipshitz, Stanley; Heal, Michael K.; Vanderkooy, John, *An Investigation of Sound Radiation by Loudspeaker Cabinets*, AES 90th Convention, Paris, France, 1991 February 19–22.

[2] Toole, Floyd E.; Olive, Sean E., *The Modification of Timbre by Resonances: Perception and Measurement*, JAES Volume 36 Issue 3 pp. 122-142; March 1988

[3] Efren Fernandez Grande, *Sound Radiation from a Loudspeaker Cabinet using the Boundary Element Method*, Master Thesis, Technical University of Denmark (DTU), September 30, 2008.

[4] Kevin J. Bastyr and Dean E Capone, *On the Acoustic Radiation from a Loudspeaker's Cabinet*, J. Audio Eng. Soc., Vol. 51, No. 4, 2003 April

[5] Mattia Cobianchi and Martial Rousseau, *Modelling the Sound Radiation by Loudspeaker Cabinets*, Comsol Conference, Cambridge (UK), September 18, 2014

[6] *Comsol 5.0 Acoustic Module Reference Manual*

[7] W. Marshall Leach Jr., *Introduction to Electroacoustics and audio amplifier design*, Dubuque, Iowa: Kendall/Hunt, 2001, ISBN 9-780757-503757.

[8] David Henwood, Gary Geaves, *Finite Element Modelling of a Loudspeaker, Part 1: Theory and Validation*, *AES 119th Convention*, New York, NY, USA, 2005 October 7–10

[9] John Vanderkooy, Paul M. Boers and Ronald M. Aarts, *Direct-Radiator Loudspeaker Systems with High-Bl*, *AES 114th Convention*, 2003 March 22–25 Amsterdam, The Netherlands

[10] D.W. Herrin, F. Martinus, T.W.Wu and F. Seybert, *A New Look at the High Frequency Boundary Element and Rayleigh Integral Approximations*, SAE, 2003